Interaction of rare-gas-containing molecules with nitrogen : þÿ M a t r i x - i s o l a t i o n a n d a b i n i t i o s t u d y o f H A r F " ï N , , þÿ H K r C l " ï N , c o m p l e x e s

Lignell, Antti

American Institute of Physics
2003-06-22

Journal of Chemical Physics June 22, 2003 Volume 118, Issue 24, pp. 11120-11128

http://link.aip.org/link/?JCP/118/11120/1

Interaction of rare-gas-containing molecules with nitrogen: Matrix-isolation and *ab initio* study of $HArF\cdots N_2$, $HKrF\cdots N_2$, and $HKrCl\cdots N_2$ complexes

Antti Lignell,[a] Leonid Khriachtchev, Mika Pettersson, and Markku Räsänen
Laboratory of Physical Chemistry, P.O. Box 55, FIN-00014, University of Helsinki, Finland

(Received 19 February 2003; accepted 26 March 2003)

The complexes of HArF, HKrF, and HKrCl with nitrogen molecules have been studied computationally and experimentally. With the help of computations the experimental data can be interpreted as showing the presence of two complex configurations, one linear and one bent. Vibrational properties of the studied molecules are very sensitive to the intermolecular interactions and complexation induces an exceptionally large blueshift (>100 cm^{-1} for HKrCl) to the H–Ar and H–Kr stretching frequency, especially for the linear configurations. The interaction energies without zero-point energy correction are between 400 and 800 cm^{-1}. According to the energy decomposition scheme, the electrostatic forces provide the most important interaction in the linear complex configurations. For the bent complexes, electrostatic and dispersion forces are competing as a leading attractive interaction. © *2003 American Institute of Physics.* [DOI: 10.1063/1.1575198]

I. INTRODUCTION

Intermolecular interactions are of central importance in many fields of chemistry, physics and biology. The vibrational properties of molecules are very sensitive to the intermolecular interactions and vibrational spectroscopy has been traditionally used to study complexation and solvation of molecules. The hydrogen stretching vibration frequency usually shifts down upon complexation and the magnitude of the shift reflects the strength of the interaction.[1] Currently, there is increasing interest in somewhat exceptional blueshifted systems where the frequency of the vibration shifts up (in energy) upon complexation (for example, $C_6H_6\cdots HCCl_3$, $F_3CH\cdots H_2O$, and $F_3CH\cdots H_2CO$).[2] In a recent theoretical study, it was suggested that the physical origin of a blueshift is based on the same mechanisms as that of a redshift: an interplay between attractive electrostatic forces, Pauli repulsion and orbital interactions.[3] It was concluded that the orbital interactions are stronger in the redshifting case causing lengthening of the bond and hence lowering of the frequency. Recently, we have reported a large experimental blueshift of more than 100 cm^{-1} for the H–Kr stretching frequency in HKrCl upon complexation with N_2.[4] HKrCl is a member of the family of hydrogen-containing rare gas compounds.[5–7] With a strong $(HKr)^+Cl^-$ ion pair character, it has a large dipole moment of 7.4 D (computationally) and therefore it is a good species to investigate electrostatic interactions with surrounding. Complexation of HXeOH with water represents another case of strong blueshifting (>100 cm^{-1}) interactions within this family of molecules.[8] In the light of these results and computations on the related $XeH_2\cdots H_2O$ system,[9] it seems that for these rare gas containing compounds the blueshift of the H–Rg stretching vibration is a normal effect. Very recently, McDowell have found computationally that $HArF\cdots CO$ and $HArF\cdots N_2$ show a blueshift of the H–Ar stretching frequency as well but the same vibration shows a redshift in the $HArF\cdots P_2$ complex.[10,11] This suggest that HRgY complexes are very attractive for understanding factors that determine whether blueshift or redshift occurs. In this paper, we report experimental and computational results for nitrogen complexes of HArF, HKrF, and HKrCl. In all the cases, complexation induces a substantial blueshift of the H–Rg stretching vibration.

II. EXPERIMENT

A. Experimental details

To prepare $HF/N_2/Rg$ matrices, a mixture of Ar (99.9999%, Aga) or Kr (99.95%, Air Liquide) with N_2 (99.9999%, Aga) was passed over an HF–pyridine polymer (Fluka) kept in a deposition line at room temperature. The [Rg]/[HF] ratio was estimated to be ~2000 based on the gas-phase integrated absorptivity of HF and the matrix thickness,[7,12] the $[N_2]/[Rg]$ being (0–1):500. For preparation of $HCl/N_2/Kr$ matrices, HCl (99%, CIL), N_2 and Kr gases were mixed in various proportions in a glass bulb. The matrix ratios used were $[HCl]/[N_2]/[Kr]=1:(0-10):1000$. The samples were deposited onto a CsI substrate kept at 20–28 K in a closed-cycle helium cryostat (APD, DE 202A). The typical matrix thickness was 100–200 μm. The spectra were measured at 7.5 K by a Nicolet 60 SX Fourier-transform infrared (FTIR) spectrometer with 0.25 or 1 cm^{-1} resolution in the middle infrared region by using a Ge–KBr beam splitter and a MCT detector.

The $HF/N_2/Rg\,(Rg=Ar,Kr)$ matrices were photolyzed with a Kr plasma discharge lamp (Opthos) emitting radiation at 127–160 nm resulting in 10–20% decomposition of the precursors in approximately 1 h and then the photolysis rate essentially decreased. The slowing down of the decomposition is probably caused by self-limitation of the photolysis,

[a]Electronic mail: lignell@csc.fi

due to the rising absorptions of the photolysis products.[13] The $HCl/N_2/Kr$ samples were photolyzed with an ArF-excimer laser (MPB, MSX-250) operating at 193 nm. The degree of decomposition of $HCl\cdots N_2$ complex after $\sim 10^4$ pulses with $\sim 10\ mJ\,cm^{-2}$ energy density was >50% and the self-limitation of photolysis due to KrCl absorption also takes place here.[14] After the irradiation, the samples were annealed up to 34 K (Ar) or 39 K (Kr).

B. HRgY monomers

HArF, HKrF, and HKrCl monomers have been studied previously.[5–7,15–19] The IR absorption spectra of these species in the H–Rg stretching region are shown in Fig. 1. A specific feature of the HArF and HKrF molecules is the experimental evidence for two groups of matrix sites with different thermal stability, and we call these site groups thermally stable ($HRgF^S$) and unstable ($HRgF^U$).[7,15] The decomposition of the thermally unstable matrix sites occurs at ~27 K and 31 K in Ar and Kr, respectively [see Figs. 1(a) and 1(b)] and the corresponding vibrational frequencies are given in Table I. This annealing-induced transformation of the matrix site structure was experimentally connected with thermal relaxation of local matrix morphology.[15] The simulations suggest that the stable and unstable configurations correspond to HArF and HKrF molecules in single and double substitutional sites with different thermal stability.[7,20] In contrast, HKrCl seems to occupy only one matrix-site configuration, and no thermal relaxation for it is found experimentally.[16–19]

C. $HArF\cdots N_2$

After deposition of a $HF/N_2/Ar\,(1{:}4{:}2000)$ mixture at 20 K, the absorption band of $HF\cdots N_2$ complex at 3881.5 cm^{-1} dominates in the IR absorption spectra [see Fig. 2(a) lower trace],[21–23] and an additional band at 3886.8 cm^{-1} appear near the $HF\cdots N_2$ band. According to our best knowledge, this band at 3886.8 cm^{-1} has not been previously reported. A probable explanation of the band is another matrix site of the $HF\cdots N_2$ (in analogy with HF monomers) or less probably a complex of hydrogen fluoride with two nitrogen molecules. HF monomer (3962.5 and 3952.4 cm^{-1}) and $(HF)_2\cdots N_2\,(3788.0\,cm^{-1})$ were also present in the sample.[21,22,24,25] We estimated by *ab initio* calculations [MP2(full)/6-311++G(2*d*,2*p*)] that the absorption intensity of $HF\cdots N_2$ is 3.5 times larger than that of the HF monomer. Based on this, the $[HF\cdots N_2]/[HF]$ ratio in our experiment is estimated to be ~2 (assumed $[HF]/[N_2]=1{:}4$).

Irradiation with the Kr plasma discharge lamp during 1 h decomposed 10–20% of $HF\cdots N_2$. After annealing of the photolyzed sample at 21 K, the known bands of $HArF^U$ (1965.7, 1969.4, and 1972.3 cm^{-1}) and $HArF^S$ (2016.3 and 2020.8 cm^{-1}) appeared in the H–Ar stretching region.[6,15] In addition to the known bands of HArF monomer, a number of new bands are seen in the N_2 doped matrices. In the H–Ar stretching region, these bands are at 2002.2 and 2029.7 cm^{-1} [see Fig. 3(a)]. In the H–Ar–F bending vibration region, an additional band at 680.3 cm^{-1} locates close to the $HArF^U$ monomer band at 686.9 cm^{-1} [see Fig. 3(b)], and a very weak band is seen also in the Ar–F stretching region at 431.7 cm^{-1} close to the $HArF^U$ monomer band (435.7 cm^{-1}). These new nitrogen-induced bands are assigned to the N_2 complexes of $HArF^U$ [see Figs. 3(a) and 3(b), and Table I]. Annealing of the sample at 32 K decomposes $HArF^U$ and its N_2 complex. New bands rise in the H–Ar stretching vibration region at 2040.8, 2091.4, 2111.6, and 2120.8 cm^{-1} blue-shifted from the bands of $HArF^S$. In the bending region a band at 702.9 cm^{-1} appears close to the $HArF^S$ bending vibrations at 693.5 and 697.0 cm^{-1} [see Figs. 3(c) and 3(d), and Table I]. These nitrogen-induced bands growing at 32 K

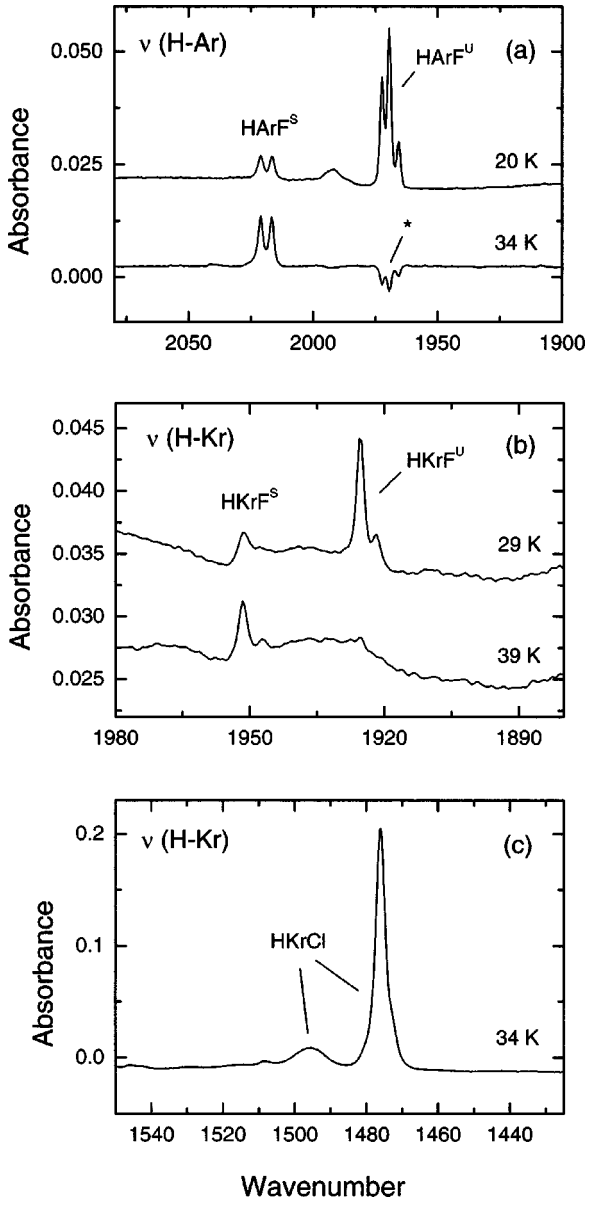

FIG. 1. IR absorption bands of (a) HArF in solid Ar, (b) HKrF in solid Kr, and (c) HKrCl in solid Kr. The samples were prepared using UV photolysis of matrix-isolated precursors (HF and HCl) followed by annealing. HArF and HKrF exhibit sites with different thermal stability (Refs. 7 and 15). Annealing above 27 K and 31 K destroys unstable sites of HArF and HKrF and increases stable matrix sites. HKrCl is found only in one matrix site. All traces are difference spectra giving the result of annealing. The small amount of HArF present after irradiation (Refs. 6 and 15) causes the negative band marked with an asterisk. The spectra are measured at 7.5 K.

TABLE I. Experimental and computational vibrations of HRgY monomers and HRgY···N_2 complexes (in cm^{-1}). The computational data are obtained with the MP2 method and various basis sets. The experimental values of the complexes are monomer-to-complex shifts. The thermally stable and unstable matrix sites are marked with S and U. IR absorption intensities are given in parentheses (in km mol^{-1}). The absorption intensity marked with an asterisk is due to coincidentally close frequencies of H–Ar stretching and N–N stretching vibration modes.

N_2+HArF	ν(H–Ar)	δ(H–Ar–F)	ν(Ar–F)	ν(N–N)
HArF and N_2 monomers				
6-311++G(2*d*,2*p*)	2148.7(1150)	743.1(82)	480.4(267)	2179.0(0)
aug-cc-pVDZ	2227.4(1170)	707.8(66)	458.2(272)	2161.3(0)
aug-cc-pVTZ	2312.8(886)	748.8(59)	481.0(266)	2220.2(0)
Experimental	(U) 1965.7, 1969.4, 1972.3	686.9, 689.3	435.7	
	(S) 2016.3, 2020.8	693.5, 697.0		
Linear complex				
6-311++G(2*d*,2*p*)	+155.2(82)	−4.0(53)	−33.1(321)	+1.3(5.9)
aug-cc-pVDZ	+152.8(29)	+41.9(34), +41.5(32)	−33.7(309)	+2.0(7.6)
aug-cc-pVTZ	+156.4(3)	+69.5(62)	−37.6(315)	+2.3(7.6)
Experimental	(U) +60.3			
	(S) +75.1, (+95.3, +104.5 weak)	+9.3, +11.8		
Bent complex				
6-311++G(2*d*,2*p*)	+34.2(658), +31.6(317)	−7.9(26), −7.0(29)	−7.3(254)	+1.3(316.6)*
aug-cc-pVDZ	+36.8(975)	−14.4(33), −7.1(35)	−7.4(255)	+2.2(1.3)
aug-cc-pVTZ	+28.1(750)	−15.0(29), −8.5(31)	−8.9(252)	+1.1(0.8)
Experimental	(U) +32.8	−6.6	−4.2	
	(S) +24.5			
N_2+HKrF	ν(H–Kr)	δ(H–Kr–F)	ν(Kr–F)	ν(N–N)
HKrF and N_2 monomers				
6-311++G(2*d*,2*p*)	2138.3(634)	679.4(20)	438.8(304)	2179.0(0)
aug-cc-pVDZ	2181.0(647)	698.6(19)	447.2(216)	2161.3(0)
aug-cc-pVTZ	2253.1(516)	735.1(17)	467.9(213)	2220.2(0)
Experimental	(U) 1925.4, 1921.7	645.9	414.1	
	(S) 1951.6	650.9		
Linear complex				
6-311++G(2*d*,2*p*)	+64.8(214)	+26.6(20)	−10.9(229)	−0.1(2.4)
aug-cc-pVDZ	+62.3(214)	+25.4(9), 25.5(9)	−14.0(245)	−0.7(2.5)
aug-cc-pVTZ	+87.7(78)	+71.2(9), +70.7(8)	−16.4(245)	+0.1(3.0)
Experimental				
	(S) +17.8[a]			
Bent complex				
6-311++G(2*d*,2*p*)	+15.8(72)	−8.5(9), −4.1(11)	−5.4(196)	+1.1(0.1)
aug-cc-pVDZ	+15.5(579)	−10.8(9), −4.9(10)	−6.8(206)	+1.3(1.6)
aug-cc-pVTZ	+10.1(467)	−9.1(8), 6.4(9)	−7.2(204)	+0.2(0.8)
Experimental	(U) +11.1			
	(S) +6.8			
N_2+HKrCl	ν(H–Kr)	δ(H–Kr–Cl)	ν(Kr–Cl)	ν(N–N)
HKrCl and N_2 monomers				
6-311++G(2*d*,2*p*)	1828.4(2412)	600.3(38)	278.5(122)	2179.0(0)
aug-cc-pVDZ	1918.4(2414)	601.0(41)	276.8(118)	2161.3(0)
aug-cc-pVTZ	1946.4(1941)	629.6(34)	288.9(123)	2220.2(0)
Experimental	1476.1	543.7, 542.1		
Linear complex				
6-311++G(2*d*,2*p*)	+145.7(907)	+29.4(42)	−11.3(141)	−1.6(2.7)
aug-cc-pVDZ	+146.3(740)	+32.8(22), +32.5(23)	−12.6(139)	−1.7(2.0)
aug-cc-pVTZ	+194.5(317)	+101.1(20), +100.2(21)	−17.6(143)	−1.2(3.6)
Experimental	+112.9			
Bent complex				
6-311++G(2*d*,2*p*)	+31.0(2189)	−5.4(19), −2.7(21)	−3.3(119)	−0.4(0.3)
aug-cc-pVDZ	+31.6(2162)	−10.3(21), −3.9(22)	−3.2(120)	−0.2(0.2)
aug-cc-pVTZ	+25.9(1765)	−8.3(17), −5.5(18)	−4.4(119)	−1.4(0.3)
Experimental	+32.4	−2.2		

[a]This band is also possible to assign to another (additional) matrix site of the bent complex.

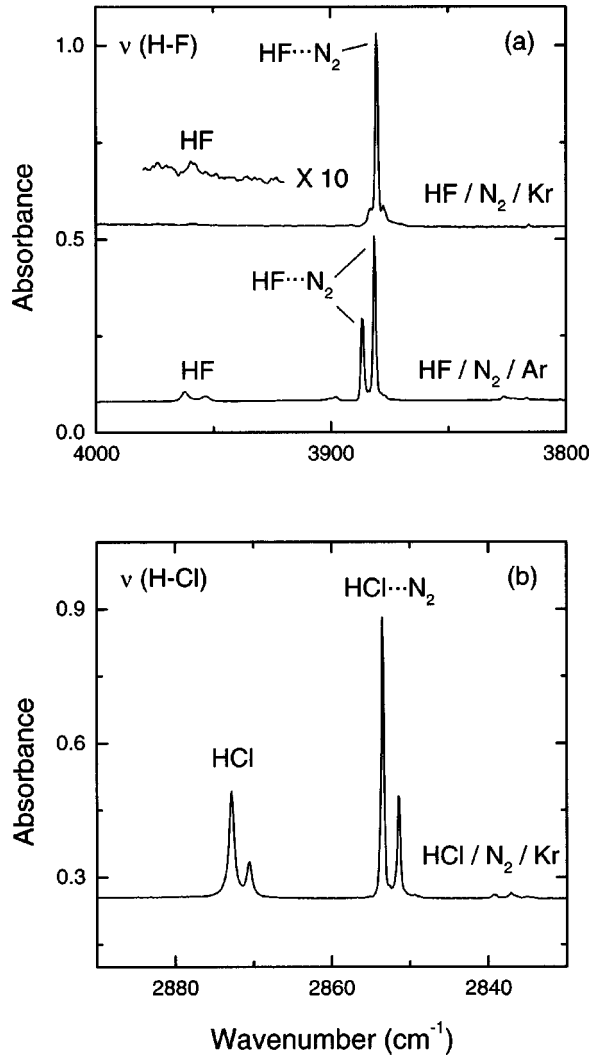

FIG. 2. FTIR spectra of (a) HF/N_2 in Kr and Ar matrices and (b) HCl/N_2 in Kr matrix at 7.5 K (see text for details).

are assigned to the $HArF^S\cdots N_2$ complexes. All these complex bands are observed only in matrices containing N_2. Upon annealing, the N_2-induced bands and HArF monomer bands grow and decompose quite simultaneously. Photostability of the complex and monomer bands is similar as checked at 193 nm irradiation.

D. $HKrF\cdots N_2$

After deposition of the $HF/N_2/Kr$ (1:4:2000) mixture at 28 K, the $HF\cdots N_2$ complex band at 3880.5 cm^{-1} dominated in the spectrum [see Fig. 2(a), the upper trace]. The estimated $[HF\cdots N_2]/[HF]$ ratio, based on the *ab initio* intensities, is ~4 in the $[HF]/[N_2]=1:4$ (estimate) experiments. After annealing a photolyzed sample at 31 K, the known bands of $HKrF^U$ (1925.6 cm^{-1}) and $HKrF^S$ (1951.6 cm^{-1}) in the H–Kr stretching region appeared in the spectra.[7] A strong additional band at 1936.5 cm^{-1} is observed upon doping with nitrogen [see Fig. 4(a)] and we assign it to the $HKrF^U\cdots N_2$ complex. The weaker band at 1926.1 cm^{-1} [marked with M^U in Fig. 4(a)] is assigned to the HKrF monomer, shifted due to the perturbed local matrix morphology upon doping with N_2.[4] When the matrices were annealed at 38 K, $HKrF^U$ and its N_2 complexes decomposes completely. Simultaneously, additional N_2-induced bands at 1958.7 and 1969.4 cm^{-1} grew [see Fig. 4(b)]. These bands are assigned to the $HKrF^S\cdots N_2$ complex (see Table I). In these experiments, we could not observe bands of HKrF or its N_2 complex in the bending region due to the low absorption intensity of the bending modes.[7,26] Again, the bands assigned to the N_2 complexes appear only upon N_2 doping. Upon annealing, the complex and corresponding monomer grows simultaneously and their photostability is similar under 193 nm irradiation.

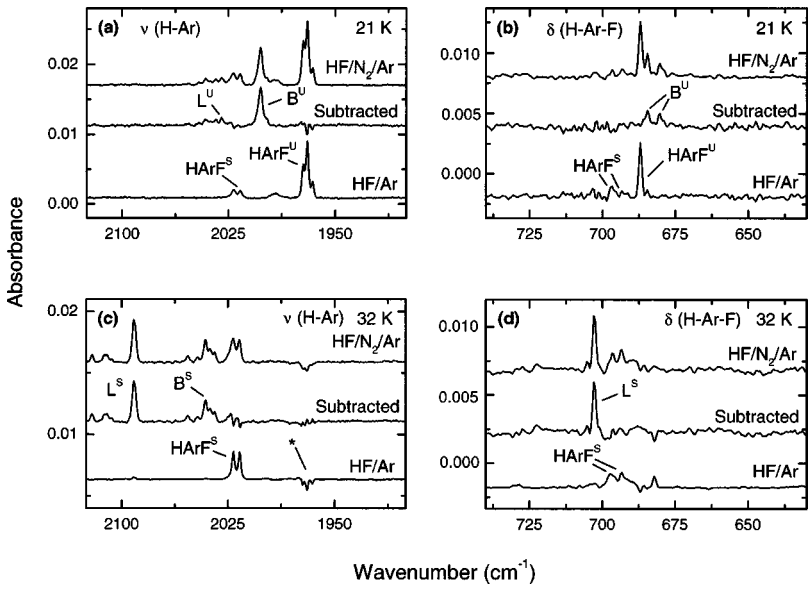

FIG. 3. FTIR spectra of HArF and $HArF\cdots N_2$ in solid Ar at 7.5 K. The samples were prepared by VUV photolysis and annealing of HF/Ar (the lower trace of each panel) and $HF/N_2/Ar$ (the upper trace of each panel) matrices. The middle trace of each panel is prepared by subtracting the monomer bands from the sum spectrum hence representing only the complex bands. The matrices are annealed at 21 K (a), (b) and 32 K (c), (d). The N_2-induced bands are assigned to the linear complex of thermally unstable HArF (L^U), the linear complex of thermally stable HArF (L^S), the bent complex of thermally unstable HArF (B^U), and the bent complex of thermally stable HArF (B^S). Annealing of the matrix above 27 K destroys thermally unstable HArF and its N_2 complex bands. All traces are difference spectra giving the result of annealing. The small amount of HArF present after irradiation causes the negative band marked with an asterisk.

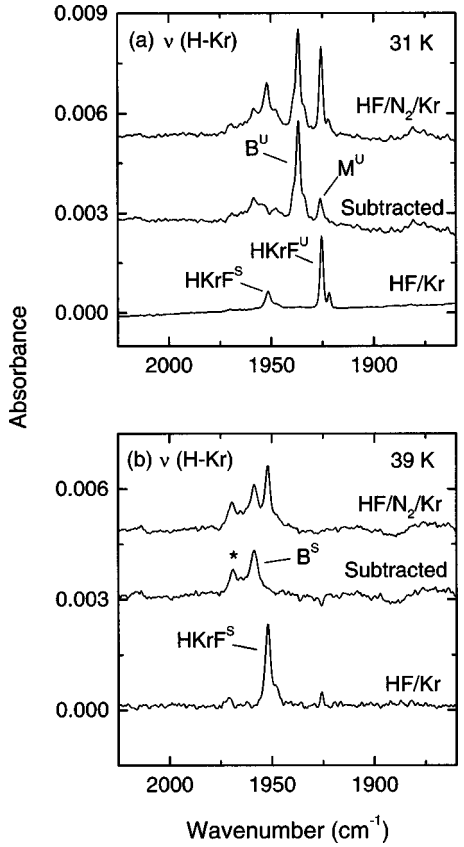

FIG. 4. FTIR spectra of HKrF monomer (the lowest trace) and HKrF···N_2 complex bands (the upper trace) at 7.5 K. The samples were prepared by photolysis and annealing of HF/Kr and HF/N_2/Kr matrices at 31 K (a) and 39 K (b). The middle traces are prepared by subtracting monomer bands from the sum spectrum hence representing only the complex bands. The N_2-induced bands are assigned to the bent complex of thermally unstable HKrF (B^U), and the bent complex of thermally stable HKrF (B^S). The band marked with an asterisk is either the linear $HKrF^S$ complex or second matrix site of the bent $HKrF^S$ complex. Annealing the matrix above 31 K destroys the $HKrF^U$ and $HKrF^U$···N_2 bands. The M^U band is assigned to the HKrF monomer perturbed by N_2 in a local matrix surrounding. Due to low absorption intensity of the bending vibrations, only the bands in the H–Kr stretching vibration region were detected in the spectra.

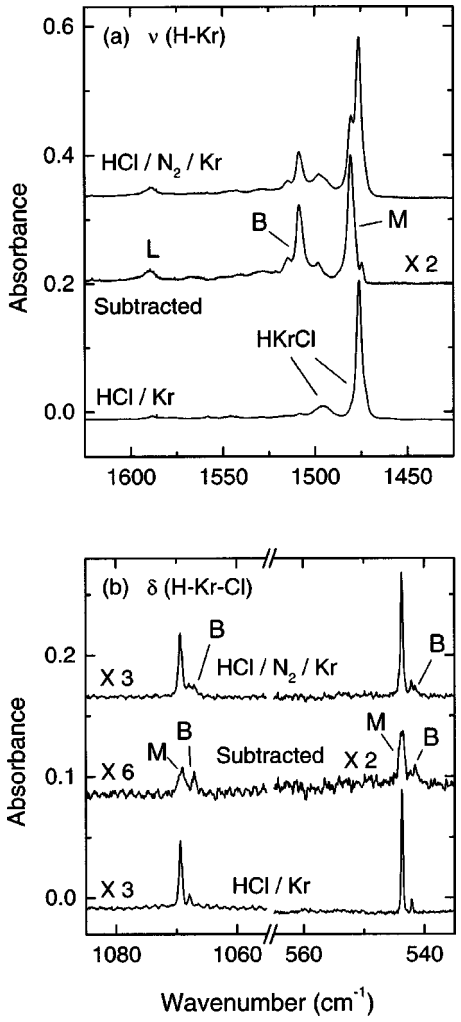

FIG. 5. FTIR spectra of HKrCl and its N_2 complexes at 7.5 K. The species are prepared by irradiating HCl/Kr and HCl/N_2/Kr matrices at 193 nm and annealing at 34 K. The middle trace of each plot is prepared by subtracting monomer bands from the sum spectrum representing only the complex bands. HKrCl does not exhibit thermally unstable matrix sites. The N_2-induced bands are assigned to the linear complex of HKrCl (L), the bent complex of HKrCl (B), and the HKrCl monomer perturbed by N_2 in a local matrix surrounding (M).

E. HKrCl···N_2

The absence of thermally unstable matrix sites makes analysis of the HKrCl···N_2 complex more straightforward compared with the HRgF complexes.[4] After deposition at 27 K ([HCl]/[N_2]/[Kr]=1:2:1000), the HCl···N_2 bands at 2853.6 and 2851.2 cm^{-1} are strong in the spectra [see Fig. 2(b)]. The computational [MP2(full)/6-311++G(2*d*,2*p*)] IR intensity of HCl···N_2 is four times larger compared with the HCl monomer,[4] and the [HCl···N_2]/[HCl] ratio is estimated to be ~0.4 for the matrix with [HCl]/[N_2]/[Kr] =1:2:1000. Annealing at 34 K of the photolyzed HCl/N_2/Kr matrices yields a number of IR absorption bands. The known HKrCl monomer bands are at 1476.1 cm^{-1} [ν(H–Kr)], 543.7, 542.1 [δ(H–Kr–Cl)], and 1069.3, 1067.9 cm^{-1} [2δ(H–Kr–Cl)].[4,16,17] In addition, nitrogen-induced bands at 1480.2, 1497.7, 1508.5, 1514.5, and 1589.0 cm^{-1} in the H–Kr stretching region, 541.5 and 1067.0 cm^{-1} in the H–Kr–Cl bending and bending overtone regions, respectively, are seen (see Fig. 5 and Table I). These nitrogen-induced bands are assigned to HKrCl···N_2 complexes as discussed previously.[4] For all the studied systems (HArF···N_2, HKrF···N_2, and HKrCl···N_2), the possible assignment of the observed spectral features to the higher order HRgY···$(N_2)_x$ ($x>1$) complexes was ruled out by the experiments with extensive N_2 doping.

III. COMPUTATIONS

A. Computational details

The quantum chemical *ab initio* calculations on the HRgY···N_2 complexes were carried out with the GAUSSIAN 98 (Revision A.9) program package on the SGI Origin 2000 computer (CSC-Center for Scientific Computing Ltd., Espoo).[27] The electron correlation method was the second order Møller–Plesset perturbation theory (MP2) taking all electrons explicitly into correlation calculations. The used basis sets were the standard split-valence 6-311+

TABLE II. Computational geometries of HRgY monomers and HRgY···N_2 complexes obtained at the MP2(full) level with various basis sets. The coordinates are presented in Fig. 6. Angles are in degrees and distances in Å.

	Bent N_2 complex					
	∠(YRgN1)	∠(RgN1N2)	r (HRg)	r (RgY)	r (RgN1)	r (N1N2)
HArF						
6-311++G(2d,2p)	66.1	136.5	1.322	2.004	3.252	1.112
aug-cc-pVDZ	66.6	139.0	1.332	2.031	3.169	1.131
aug-cc-pVTZ	66.9	142.4	1.314	1.984	3.140	1.109
HKrF						
6-311++G(2d,2p)	62.0	138.0	1.465	2.081	3.406	1.112
aug-cc-pVDZ	63.2	140.1	1.474	2.066	3.301	1.131
aug-cc-pVTZ	63.2	143.7	1.451	2.032	3.274	1.109
HKrCl						
6-311++G(2d,2p)	72.0	149.1	1.495	2.558	3.387	1.113
aug-cc-pVDZ	72.0	150.6	1.496	2.573	3.286	1.131
aug-cc-pVTZ	71.0	154.9	1.480	2.507	3.264	1.110
	Linear N_2 complex					
	∠(N2N1H)	∠(N1HRg)	r (HRg)	r (RgY)	r (N1H)	r (N1N2)
HArF						
6-311++G(2d,2p)	180.0	180.0	1.314	2.027	2.149	1.112
aug-cc-pVDZ	180.0	180.0	1.325	2.061	2.094	1.130
aug-cc-pVTZ	180.0	180.0	1.306	2.013	2.053	1.109
HKrF						
6-311++G(2d,2p)	180.0	180.0	1.461	2.090	2.415	1.113
aug-cc-pVDZ	179.2	177.3	1.471	2.074	2.386	1.131
aug-cc-pVTZ	179.1	177.6	1.445	2.043	2.248	1.110
HKrCl						
6-311++G(2d,2p)	180.0	180.0	1.485	2.575	2.349	1.113
aug-cc-pVDZ	179.2	177.2	1.486	2.595	2.284	1.131
aug-cc-pVTZ	178.9	177.6	1.465	2.537	2.195	1.110
	Monomer					
	r (HRg)	r (RgY)	r (NN)			
HArF						
6-311++G(2d,2p)	1.326	1.996				
aug-cc-pVDZ	1.337	2.022				
aug-cc-pVTZ	1.317	1.975				
HKrF						
6-311++G(2d,2p)	1.467	2.075				
aug-cc-pVDZ	1.477	2.058				
aug-cc-pVTZ	1.453	2.024				
HKrCl						
6-311++G(2d,2p)	1.500	2.551				
aug-cc-pVDZ	1.501	2.567				
aug-cc-pVTZ	1.484	2.500				
N_2						
6-311++G(2d,2p)			1.113			
aug-cc-pVDZ			1.131			
aug-cc-pVTZ			1.110			

$+G(2d,2p)$ and augmented Dunning's correlation consistent valence double- and triple-zeta basis sets aug-cc-pVXZ (X =D,T). The natural population analysis (NPA) at the MP2 level was used to find partial charges of atoms in the complexes. The Morokuma interaction energy component analysis for the complexes was carried out with Gamess program library.[28–30] The Morokuma analysis was run at the Hartree–Fock (HF) level by using the aug-cc-pVDZ basis set at the optimized geometries (MP2/aug-cc-pVDZ). The basis sets for the Gamess calculation were taken from the basis function database.[31] The dispersive interaction was estimated as a difference of electronic interaction energies obtained at the

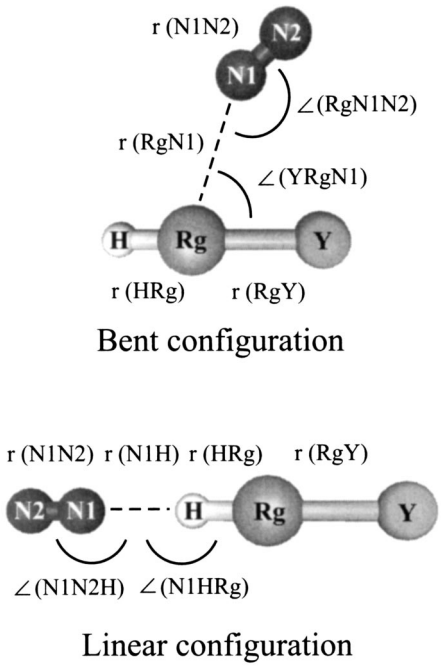

FIG. 6. Computational structures of the linear and bent configurations of the $HRgY\cdots N_2$ complexes. The geometry parameters calculated at various theory levels are presented in Table II.

MP2 and HF levels by using the same complex geometry $[\Delta E(\text{disp})=\Delta E(\text{MP2})-\Delta E(\text{HF})]$.[32,33] The interaction energies of the complexes were calculated by using Counterpoise basis set superposition error (BSSE) correction.[34]

B. Computational results

The structures of the complexes obtained at three computational levels are presented in Table II and the notations are given in Fig. 6. For all complexes studied, we found two configurations corresponding to the true energy minima on intermolecular potential energy surface. Following Ref. 4, we call them linear and bent complexes (see Fig. 6). As a general trend, the complexation leads to a shortening of the H–Rg bond and an elongation of the Rg–Y bond compared with the monomer. The computational harmonic vibrational frequencies and IR absorption intensities are presented in Table I. The vibrational frequencies of the complexes are given as monomer-to-complex shifts, and the experimental values are obtained using the strongest monomer and complex bands. Our results on $HArF\cdots N_2$ (linear configuration) agree with the corresponding computational data very recently presented by McDowell.[11] The computational electronic interaction energies and vibrational zero-point energy (ZPE) corrected interaction energies are presented in Table III. The interaction energy of $HArF\cdots N_2$ is the largest, HKrF and HKrCl complexes having smaller interaction energies. As suggested by the ZPE corrected values, the bent configuration of HKrF and HKrCl complexes is energetically more favorable than the corresponding linear configuration. The situation is less definite for HArF where two of the three levels of theory feature a larger stability of the linear configuration. The results of the Morokuma interaction energy component analysis at the HF/aug-cc-pVDZ level are presented in Table IV. The electrostatic energy provides the largest contribution in the attractive interaction energy of the linear complexes. For the bent complexes, the estimated dispersion energy component is comparable with the electrostatic contribution. The charge-transfer and polarization energy components are also important, especially in the linear configurations.

TABLE III. Electronic interaction energies and vibrational ZPE-corrected electronic interaction energies of $HRgY\cdots N_2$ complexes obtained at various computational levels. The ZPE corrected energies are presented in parentheses. The values are in cm^{-1}.

	MP2(full)/ 6-311++(2*d*,2*p*)	MP2(full)/ aug-cc-pVDZ	MP2(full)/ aug-cc-pVTZ
HArF			
Linear	711.1 (487.0)	790.3 (538.3)	783.3 (430.2)
Bent	507.1 (356.8)	573.2 (426.4)	636.0 (488.8)
HKrF			
Linear	441.7 (224.9)	424.0 (260.8)	393.8 (123.9)
Bent	454.5 (332.3)	470.4 (338.9)	546.1 (410.1)
HKrCl			
Linear	471.5 (234.2)	496.7 (284.0)	442.2 (88.9)
Bent	495.1 (366.8)	529.2 (395.7)	612.5 (463.3)

IV. DISCUSSION

A. Nature of the interaction

The bonding in the HRgY molecules consists mainly of the ionic $(HRg)^+Y^-$ and covalent HRgY parts. At the equilibrium geometry, the ionic contribution is dominant.[5,35] The strong $(HRg)^+Y^-$ character explains the large computational dipole moments (up to 9 D),[5] comparable with salt molecules. The dipole moments of the presently studied molecules are 7.2 D for HArF, 6.5 D for HKrF, and 7.4 D for HKrCl as calculated at the MP2(full)/6-311++G(2*d*,2*p*) level. As mentioned earlier, these large dipole moments make the HRgY molecules very sensitive probes for studying electrostatic and induction interactions. According to a simple electrostatic analysis on the $HKrCl\cdots N_2$ system presented in our previous paper, the interaction energy is mainly composed of dipole–quadrupole and dispersive components in both linear and bent complex configurations.[4]

In accordance with this analysis, the Morokuma interaction energy decomposition scheme (see Table IV) shows that the electrostatic interaction between frozen charge distributions of the complex partners E_{ES} is an important component of the attractive interaction in both forms of complexes. The orbital relaxation energy, which is the energy difference when the orbitals of the separate complex partners are changed to the molecular orbitals of the complex, gives an important contribution to the total interaction energy. Its magnitude is larger in the linear than in the bent complexes. The orbital relaxation energy can be split into the polarization E_{PL} and charge-transfer E_{CT} terms. The polarization E_{PL} originates from mixing of occupied and nonoccupied orbitals of the same complex partner. The charge-transfer terms originate from mixing of occupied orbitals of the one complex partner with the nonoccupied orbitals of the other partner.

The magnitudes of E_{PL} and E_{CT} contributions are comparable to each other. The polarization energy in both configurations of the complexes and the charge-transfer energy in the linear complexes are mainly contributed by the N_2 moieties. In the bent complexes, the charge-transfer energies influenced by HRgY moieties are dominant. The estimated dispersion energy component is larger for the bent complexes and it is comparable with the E_{ES} contribution.

B. Vibrational properties

The computational complexation-induced spectral shifts are in good agreement with the experimental data. All levels of computations predict substantial blueshift for the H–Rg stretching vibration. Based on the calculations, the complex bands with larger blueshift are assigned to the linear configurations and those with smaller blueshifts to the bent configurations. The distinction between the linear and bent forms is quite straightforward for $HArF\cdots N_2$ and $HKrCl\cdots N_2$. For $HKrF\cdots N_2$, the difference in shifts of two observed bands (11.0 cm^{-1}, see asterisk in Fig. 4) is not large enough to make a decisive conclusion. These two bands may originate either from the two matrix sites of bent configurations or from the linear and bent configurations. Some overestimations of the computational H–Rg stretching frequencies occur for the linear configurations when compared with the experimental values. The larger basis set (especially aug-cc-pVTZ) gives even larger shifts, which might indicate imbalance between the correlation level and the basis set.[36] The discrepancy between the magnitudes of the calculated and observed shifts is partially due to the different matrix shifts of HRgY monomer and its N_2 complex. Often matrix shifts of complexes are smaller when compared with the corresponding monomer, lowering the absolute value of monomer-to-complex shift.[37]

The HArF and HKrF molecules and their complexes have two matrix sites with different thermal stability. In the proposed image, an HRgF molecule in the unstable matrix site reorganizes upon annealing to the more stable site.[15] This process might be connected with the initial trapping of the HF precursor in either interstitial or in single substitutional sites.[7] One remarkable observation should be mentioned here: the band of the bent HArF complex in the unstable matrix site is dominant while the linear complex is hardly visible. In the stable matrix site, the strong absorption of the linear complex is seen. This fact can be explained by thermal relaxation of the bent HArF complex to the more stable linear complex. For the HKrF, it is possible that the linear complex is not formed, and this finds the explanation in the relative energies of the linear and bent configurations (see Table III). Of course, this conclusion is very tentative. It is interesting to note that the N_2-induced longer-range perturbed sites of the HRgY monomers [M in Figs. 4(a) and 5(a), 5(b)] are present only in the krypton matrices. This suggests a larger nitrogen-induced perturbation for the krypton lattice when compared with argon.

The complexation of HRgY molecules with N_2 leads to a shortening of the hydrogen donor (H–Rg) bond and elongation of the Rg–Y bond. This effect is stronger in the linear complexes increasing efficiently charge separation of the $(HRg)^+Y^-$ complex partner. As a result, the HRg moiety structurally approaches the $(HRg)^+$ cation,[38,39] indicated by shortening of the H–Rg bond length and increase of the H–Rg stretching frequency. This is opposite to ''classical'' hydrogen bonding effects where the proton donor (H–X) bond in a $Y\cdots H–X$ system (Y is proton acceptor) elongates and the corresponding stretching vibration frequency redshifts. It has been described that the origin of the blueshifting hydrogen bonds can be understood by a charge transfer from the proton acceptor Y to the electronegative proton donor moieties X in the $Y\cdots H–X$ complex system.[2] This charge transfer to the larger part of the donor molecule prevents further occupancy of the antibonding σ^* orbital of the H–Y bond, which shortens the bond instead of the typical elongation. Recently, Li and co-workers have suggested that the mechanisms behind the blueshifting and redshifting hydrogen bonds are similar.[3] They noticed that electrostatic inter-

TABLE IV. Interaction energy contributions (see text for details) of the $HRgY\cdots N_2$ complexes calculated with Morokuma analysis at RHF/aug-cc-pVDZ level. The values marked in parentheses represent the proportion of the each energy component from the total attractive interaction. The values are in cm^{-1}.

	$HArF\cdots N_2$		$HKrF\cdots N_2$		$HKrCl\cdots N_2$	
	Linear	Bent	Linear	Bent	Linear	Bent
E_{ES}	(36%) −1209.3	(38%) −669.2	(39%) −606.8	(37%) −599.6	(37%) −855.3	(34%) −612.3
E_{EX}	1845.6	935.2	888.2	934.3	1348.0	1007.4
E_{PL}	(30%) −1008.3	(18%) −316.3	(18%) −286.2	(16%) −255.0	(22%) −500.2	(16%) −292.3
N_2 part	−840.2	−271.1	−247.3	−219.5	−394.4	−246.5
HRgY part	−180.2	−37.1	−71.1	−29.0	−122.2	−37.1
E_{CT}	(25%) −865.2	(13%) −224.7	(21%) −327.0	(14%) −220.6	(24%) −544.7	(12%) −217.3
N_2 part	−721.2	−104.7	−255.7	−94.2	−426.2	−81.6
HRgY part	−144.0	−120.1	−71.1	−126.4	−118.5	−135.6
E_{MIX}	637.4	174.0	162.6	153.2	321.8	191.2
$E_{\Delta-E}$	−599.6	−100.7	−169.2	12.5	−230.7	76.6
E_{ED}	(9%) −312.1	(31%) −546.5	(21%) −330.2	(36%) −573.0	(17%) −380.8	(39%) −705.6
E_{TOT}	−911.7	−647.2	−499.4	−560.5	−611.5	−339.4

E_{ES}=electrostatic energy.
E_{EX}=exchange repulsion energy.
E_{PL}=polarization energy.
E_{CT}=charge-transfer energy.
E_{MIX}=high order coupling energy.
$E_{\Delta-E}$=total interaction energy without dispersion interaction.
E_{ED}=estimated dispersion energy, calculated by int E(MP2)−int E(HF).
E_{TOT}=total interaction energy.

action with corresponding Pauli repulsion term is the natural source of the blueshift whereas the strong orbital interaction causes the elongation of the H–X bonds and hence a decrease of the vibrational frequency. These effects are competing upon complexation: ''classical'' redshifting hydrogen bonds originate from a large orbital interaction while a weaker orbital interaction (or stronger electrostatic interaction and Pauli repulsion) in complexes can result in a blueshift of the vibrational frequency. In our studies, very large blueshifts of the H–Rg stretching frequency are found for all $HRgY\cdots N_2$ complexes.

For some of the HRgY compounds, complexation may be a significant stabilizing factor. In this respect, HHeF, the computationally predicted chemically bound helium containing molecule is rather interesting.[40–42] It has been calculated that HHeF is unstable with respect to tunneling into its fragments H+He+F or HF+He and the lifetimes associated with these channels are predicted to be in a femtosecond or picosecond scale.[40,41] The tunneling rate strongly depends on the potential-barrier parameters (height and width). Thus, tunneling-induced decomposition of HHeF can be suppressed upon proper complexation (for instance, $HHeF\cdots N_2$). However, the situation is not straightforward because the destabilization via bending coordinate was found in a related system.[8] Moreover, the energy of these metastable species can be, in principle, decreased upon complexation below the atomic asymptote, which would offer a real basis for experimental preparation. Investigations on this topic are underway in our laboratory.

V. CONCLUSIONS

The complexes of HArF, HKrF, and HKrCl with nitrogen have been studied. Two complex geometries (linear and bent) are found both computationally and experimentally in low-temperature matrices for these three species with possible exclusion of a stable configuration of $HKrF\cdots N_2$ where only the bent complex seems to appear in our experiments. The H–Rg stretching frequency of these species is very sensitive to the complexation as evidenced by the large monomer-to-complex blueshifts (>100 cm^{-1} for HKrCl). The computational interaction energies of the complexes before ZPE correction are between 400 and 800 cm^{-1}. The electrostatic forces provide the most important contributions to the interaction energy of the linear $HRgY\cdots N_2$ complexes. In the bent complexes, electrostatic and dispersion forces are competing in attractive interaction energy. The complexation-introduced stabilization of the weakly bound HRgY molecules is emphasized and its potential for making HHeF observable is suggested.

ACKNOWLEDGMENTS

The Academy of Finland supported this work. The CSC-Center for Scientific Computing Ltd. (Espoo, Finland) is thanked for providing computer facilities. Dr. Jan Lundell is gratefully thanked for very useful discussions. A.L. is a member of the graduate school LASKEMO (Ministry of Education, Finland).

[1] R. M. Badger and S. H. Bauer, J. Chem. Phys. **5**, 839 (1937).
[2] P. Hobza and Z. Havlas, Chem. Rev. (Washington, D.C.) **100**, 4253 (2000), and references therein; B. J. van der Veken, W. A. Herrebout, R. Szostak, D. N. Shchepkin, Z. Havlas, and P. Hobza, J. Am. Chem. Soc. **123**, 12290 (2001); S. N. Delanoye, W. A. Herrebout, and B. J. van der Veken, *ibid.* **124**, 7490 (2002); K. Hermansson, J. Phys. Chem. A **106**, 4695 (2002).
[3] X. Li, L. Liu, and B. Schlegel, J. Am. Chem. Soc. **124**, 9639 (2002).
[4] A. Lignell, L. Khriachtchev, M. Pettersson, and M. Räsänen, J. Chem. Phys. **117**, 961 (2002).
[5] J. Lundell, L. Khriachtchev, M. Pettersson, and M. Räsänen, Low Temp. Phys. **26**, 680 (2000).
[6] L. Khriachtchev, M. Pettersson, N. Runeberg, J. Lundell, and M. Räsänen, Nature (London) **406**, 874 (2000).
[7] M. Pettersson, L. Khriachtchev, A. Lignell, M. Räsänen, Z. Bihary, and R. B. Gerber, J. Chem. Phys. **116**, 2508 (2002).
[8] A. V. Nemukhin, B. L. Grigorenko, L. Khriachtchev, H. Tanskanen, M. Pettersson, and M. Räsänen, J. Am. Chem. Soc. **124**, 10706 (2002).
[9] J. Lundell and M. Pettersson, Phys. Chem. Chem. Phys. **1**, 1691 (1999).
[10] S. A. C. McDowell, Chem. Phys. Lett. **368**, 649 (2003).
[11] S. A. C. McDowell, Phys. Chem. Chem. Phys. **5**, 808 (2003).
[12] A. S. Pine, A. Fried, and J. W. Elkins, J. Mol. Spectrosc. **109**, 30 (1985).
[13] L. Khriachtchev, M. Pettersson, and M. Räsänen, Chem. Phys. Lett. **288**, 727 (1998).
[14] M. E. Fajardo, R. Withnall, J. Feld, F. Okada, W. Lawrence, L. Wiedeman, and V. A. Apkarian, Laser Chem. **9**, 1 (1988).
[15] L. Khriachtchev, M. Pettersson, A. Lignell, and M. Räsänen, J. Am. Chem. Soc. **123**, 8610 (2001).
[16] M. Pettersson, J. Lundell, and M. Räsänen, J. Chem. Phys. **102**, 6423 (1995).
[17] A. Lignell, J. Lundell, M. Pettersson, L. Khriachtchev, and M. Räsänen, Low Temp. Phys. (to be published).
[18] L. Khriachtchev, M. Pettersson, J. Lundell, and M. Räsänen, J. Chem. Phys. **114**, 7727 (2001).
[19] L. Khriachtchev, M. Saarelainen, M. Pettersson, and M. Räsänen, J. Chem. Phys. **118**, 6403 (2003).
[20] Z. Bihary, G. M. Chaban, and R. B. Gerber, J. Chem. Phys. **116**, 5521 (2002).
[21] M. T. Bowers, G. I. Kerley, and W. H. Flygare, J. Chem. Phys. **45**, 3399 (1966).
[22] M. G. Mason, W. G. Von Holle, and D. W. Robinson, J. Chem. Phys. **54**, 3491 (1970).
[23] L. Andrews, B. J. Kelsall, and R. T. Arlinghaus, J. Chem. Phys. **79**, 2488 (1983).
[24] L. Andrews and G. L. Johnson, Chem. Phys. Lett. **96**, 133 (1983).
[25] L. Andrews and G. L. Johnson, J. Phys. Chem. **88**, 425 (1984).
[26] J. Lundell, G. M. Chaban, and R. B. Gerber, Chem. Phys. Lett. **331**, 308 (2000).
[27] M. J. Frisch, G. W. Trucks, H. B. Schlegel *et al.*, GAUSSIAN 98, Revision A.9, Gaussian, Inc., Pittsburgh, PA, 1998.
[28] K. Morokuma, J. Chem. Phys. **55**, 1236 (1971).
[29] K. Kitaura and K. Morokuma, Int. J. Quantum Chem. **10**, 325 (1976).
[30] M. W. Schmidt, K. K. Baldridge, J. A. Boatz *et al.*, J. Comput. Chem. **14**, 1347 (1993).
[31] Extensible Computational Chemistry Environment Basis Set Database, Version 10/29/02, Molecular Science Computing Facility, Environmental and Molecular Sciences Laboratory, Pacific Northwest Laboratory, P.O. Box 999, Richland, Washington 99352, and references therein.
[32] Z. Latajka, J. Mol. Struct.: THEOCHEM **251**, 245 (1991).
[33] J. Lundell, M. Räsänen, and Z. Latajka, J. Phys. Chem. **97**, 1152 (1993).
[34] S. F. Boys and F. Bernardi, Mol. Phys. **19**, 553 (1970).
[35] I. Last and T. F. George, J. Chem. Phys. **89**, 3071 (1988).
[36] N. Runeberg, M. Seth, and P. Pyykkö, Chem. Phys. Lett. **246**, 239 (1995).
[37] J. Lundell, S. Jolkkonen, L. Khriachtchev, M. Pettersson, and M. Räsänen, Chem.-Eur. J. **7**, 1670 (2001).
[38] J. W. C. Johns, J. Mol. Spectrosc. **106**, 124 (1984).
[39] C. J. H. Schutte, Chem. Phys. Lett. **353**, 389 (2002).
[40] G. M. Chaban, J. Lundell, and R. B. Gerber, J. Chem. Phys. **115**, 7341 (2001).
[41] T. Takayanagi and A. Wada, Chem. Phys. Lett. **352**, 91 (2002).
[42] M. W. Wong, J. Am. Chem. Soc. **122**, 6289 (2000).